Available online at www.sciencedirect.com
SCIENCE DIRECT®
Journal of Magnetic Resonance 170 (2004) 136–148
JMR Journal of Magnetic Resonance
www.elsevier.com/locate/jmr

A one-shot method for measurement of diffusion

Yi-Qiao Song[a,*] and Xiaoping Tang[b]

[a] Schlumberger-Doll Research, 36 Old Quarry Road, Ridgefield, CT 06877, USA
[b] Department of Physics, University of Nevada at Reno, Reno, NV 89557, USA

Received 26 February 2004; revised 7 June 2004
Available online 17 July 2004

Abstract

This paper describes an NMR method capable of determining the diffusion constant of a material within a few milliseconds and without the need of multiple scans. The method can be used with static or pulsed magnetic field gradients. It may be used to detect time-dependent processes, such as in chemical reactions, production monitoring, and medical MRI.

Keywords: Diffusion; Multiple echoes; Off-resonance effects

1. Introduction

The diffusion constant of molecules is often measured by NMR experiments using static or pulsed magnetic field gradients. The pulse sequences for such measurements are based on the work of Hahn [1] and Stejskal and Tanner [2]. The basic idea is to first use the field gradient to create a spatial sinusoidal modulation of spin magnetization in the sample, then monitor the time evolution (often decay) of the signal. The modulation is created by precession of the spin magnetization in the field gradient and often described by a wave-vector, k (or q), which is determined by the gradient g and its duration τ

$$k = \gamma g \tau. \tag{1}$$

Here, γ is the gyromagnetic ratio of the observed nuclei. The diffusion constant is obtained by a series of measurements with different values of k and for each k several scans in order to select the desired coherence pathway.

In addition, when fluid is present in a porous medium, such as a rock, the molecular diffusion can be affected by the presence of the solid [3]. As a result, the apparent diffusion constant of the fluid may be reduced when the diffusion distance approaches the size of the pores, such as the length scale defined by the surface-to-volume ratio [4]. In this case, the diffusion propagator [5,6] is often measured as a means to characterize the pore geometry. Often, data for more than 10 values of k are needed to properly define the propagator. Thus, multiple measurements are needed and the time to obtain a full data set can be very long.

The current paper introduces a method for the measurement of diffusion that uses one scan acquisition to acquire data at a series of k. It requires no additional scans for phase cycling nor for different values of k. It is thus, a truly fast measurement. This method is closely related to the previous imaging methods of PREVIEW [7] and QUEST [8], and the methods for diffusion measurements by small tipping angle pulses, such as BURST-type sequences, for example, in [9–11]. We will show that the current method is advantageous in more efficient use of the available signal (thus better signal-to-noise ratio) and not limited to small tipping angles.

2. Multiple modulations

2.1. Spatial modulation of spin magnetization

In the presence of a magnetic field gradient **g**, the transverse magnetization components, M_x, and M_y, precess to acquire a phase (Φ) that is proportional to the

* Corresponding author. Fax: 1-203-438-3819.
E-mail address: ysong@slb.com (Y.-Q. Song).

1090-7807/$ - see front matter © 2004 Elsevier Inc. All rights reserved.
doi:10.1016/j.jmr.2004.06.009

local magnetic field, $B_0 + \mathbf{g}\cdot\mathbf{r}$, where B_0 is the average field, $\mathbf{r}$ is a vector in space

$$\Phi = \tau\gamma\mathbf{g}\cdot\mathbf{r} + \tau\gamma B_0, \tag{2}$$

where τ is the time period of the precession. We omit the constant term since it is the same for the entire sample. This spatially dependent phase factor causes the magnetization to form a sinusoidal modulation in space with a spatial wave length λ

$$\frac{1}{\lambda} = \gamma|\mathbf{g}|\tau. \tag{3}$$

Often, a wave-vector $\mathbf{k}$ is defined as $\mathbf{k} = \gamma\mathbf{g}\tau$ to depict the orientation and the length scale of the modulation. Most diffusion-related measurements require several scans to generate different values of $\mathbf{k}$ and often for necessary phase cycling.

2.2. Coherence pathways

We define three states of spin magnetization of an ensemble of spin-1/2 nuclei, M_0, M_-, and M_+:

$$\begin{aligned} M_0 &= M_z, \\ M_+ &= (M_x + \mathrm{i}M_y)/\sqrt{2}, \\ M_- &= (M_x - \mathrm{i}M_y)/\sqrt{2}. \end{aligned} \tag{4}$$

These states are marked by q which can be 0, +1, and −1, (or 0, + and −), respectively. Note that the M_- and M_+ defined here are a factor of $1/\sqrt{2}$ of those in [12,13]. A RF pulse rotates the magnetization vector, $\mathbf{M} \equiv (M_+, M_-, M_0)$, and thus changes q

$$\mathbf{M}(t_p) = \mathbf{R}\cdot\mathbf{M}(0). \tag{5}$$

Here, $\mathbf{M}(0)$ and $\mathbf{M}(t_p)$ are the magnetization vectors before and after the pulse of a duration t_p. $\mathbf{R}$ depends on the Larmor frequency offset from the RF frequency ω_{RF}, $\Delta\omega_0 \equiv \gamma|B_0| - \omega_{RF}$, ω_1, and t_p. Then, the nutation frequency is $\Omega \equiv \sqrt{\omega_1^2 + \Delta\omega_0^2}$, where $\omega_1 = \gamma B_1/2$, and the tipping angle is Ωt_p. The matrix elements, $R_{l,m}(\Delta\omega_0, \omega_1, t_p, \phi)$, are shown below (note that they are slightly different from those used in [12,13] due to the definitions of $M_\pm$)

$$\begin{aligned} R_{+,+} &= R^*_{-,-} \\ &= \frac{1}{2}\left\{\left(\frac{\omega_1}{\Omega}\right) + \left[1 + \left(\frac{\Delta\omega_0}{\Omega}\right)^2\right]\cos(\Omega t_p)\right\} \\ &\quad + \mathrm{i}\left(\frac{\Delta\omega_0}{\Omega}\right)\sin(\Omega t_p), \end{aligned} \tag{6}$$

$$R_{0,0} = \left(\frac{\Delta\omega_0}{\Omega}\right)^2 + \left(\frac{\omega_1}{\Omega}\right)^2\cos(\Omega t_p), \tag{7}$$

$$\begin{aligned} R_{+,0} &= R^*_{-,0} \\ &= \frac{\omega_1}{\sqrt{2}\Omega}\left\{\frac{\Delta\omega_0}{\Omega}[1 - \cos(\Omega t_p)] - \mathrm{i}\sin(\Omega t_p)\right\}\mathrm{e}^{+\mathrm{i}\phi}, \end{aligned} \tag{8}$$

$$R_{0,+} = R^*_{0,-} = \frac{\sqrt{2}\omega_1}{\Omega}\left\{\frac{\Delta\omega_0}{\Omega}[1 - \cos(\Omega t_p)] - \mathrm{i}\sin(\Omega t_p)\right\}\mathrm{e}^{-\mathrm{i}\phi}, \tag{9}$$

$$R_{+,-} = R^*_{-,+} = \frac{1}{2}\left(\frac{\omega_1}{\Omega}\right)^2[1 - \cos(\Omega t_p)]\mathrm{e}^{+\mathrm{i}2\phi}. \tag{10}$$

In this article, we consider pulses of constant amplitude while the nutation angle (α) is varied by the pulse duration, and the rotation matrix of the lth pulse is labeled as $\Lambda_l \equiv R_{q,q'}(\Delta\omega_0, \omega_1, t_p, \phi)$, where q' and q are the magnetization states before and after the lth pulse.

The pulse sequences considered in this article consist of a train of N pulses. A coherence pathway is characterized by a series of $N+1$ numbers, $Q \equiv (q_0, q_1, \ldots, q_N)$, where $q_0 = 0$ is the magnetization state before the first pulse. The contribution of each coherence pathway can be written as a product of three factors

$$\begin{aligned} M_Q = A_Q \cdot B_Q \cdot C_Q &= \left(\prod_{l=1}^{N}\Lambda_l\right) \times \left\langle \exp\left(\mathrm{i}\sum_{l=1}^{N} q_l\varphi_l\right)\right\rangle \\ &\quad \times \exp\left[-\sum_{l=1}^{N}\left(q_l^2/T_2 + \frac{1-q_l^2}{T_1}\right)\tau_l\right], \end{aligned} \tag{11}$$

where τ_l is the time period between the lth and the $(l+1)$th pulses. A_Q is the frequency spectrum of the resulting signal and it depends only on the RF pulses. B_Q is due to diffusion and is independent of frequency. φ_l is the random phase factor due to diffusion between pulse l and $l+1$ in the presence of magnetic field gradients. The angle brackets $\langle\ldots\rangle$ represent an ensemble average of the random phase factors, $\varphi_0, \varphi_1, \ldots, \varphi_N$. C_Q is the relaxation attenuation factor and it decays with a time constant T_1 during the periods when $q_l = 0$ and with T_2 when $q_l = \pm 1$.

To understand B_Q, it is useful to introduce for each coherence pathway the instantaneous wave-vector $k(t)$ in analogy to the approach in magnetic resonance imaging [14,15]

$$k(t) = \gamma g\int_0^t q(t')\mathrm{d}t', \tag{12}$$

where g is the field gradient, $q(t')$ is the instantaneous value of q that is piecewise constant between pulses. The attenuation induced by unrestricted diffusion for a given coherence pathway can then generally be written as [2]

$$B_Q = \exp\left\{-D\int_0^T k(t)^2\mathrm{d}t\right\}, \tag{13}$$

where D is the bulk diffusion constant, and time $t = 0$ is defined as the beginning of the sequence and T is the echo time. A modified equation [16] can be used to evaluate the diffusion decay for restricted diffusion. The pulse sequences in this article are deliberately designed

so that all coherence pathways will yield echoes that are well separated in the time domain. We will show the resulting B_Q for our sequences later.

2.3. Multiple modulation multiple echoes

Consider a static magnetic field gradient and a train of three pulses with tipping angles α_1, α_2, and α_3, and the time spacing between them to be τ_1, τ_2,

$$\alpha_1\text{–}\tau_1\text{–}\alpha_2\text{–}\tau_2\text{–}\alpha_3\text{–acquisition} \tag{14}$$

The nutation angles of the pulses are *not* necessarily multiples of 90°. In the presence of constant field gradients, for instance, the nutation angle of a pulse will depend on the frequency offset and the RF uniformity so that it may not be the same for the entire sample. Neglecting recovery due to T_1 relaxation for the moment, the above sequence will allow a total of five coherence pathways to be observed and thus create five signals

phase index	q_0	q_1	q_2	q_3	b_Q	c_{1Q}	c_{2Q}
0	0	0	0	−1	0	0	0
1	0	1	0	−1	11/3	3	2
2	0	−1	1	−1	6	0	6
3	0	0	1	−1	18	1	6
4	0	1	1	−1	128/3	0	8

(15)

$q_3 = -1$ for the detection period as is the convention. The first coherence pathway (0,0,0,−1) gives rise to an FID signal and all others produce echoes. The symbols b_Q, c_{1Q}, and c_{2Q} will be explained later.

During the periods of τ_1 and τ_2, transverse magnetization ($q = \pm 1$) will acquire a phase of $qg\tau_i$ ($i = 1$ and 2), thus the echo appears when the total phase is zero

$$q_1\tau_1 + q_2\tau_2 - \tau_3 = 0, \tag{16}$$

where τ_3 is the waiting time after the last pulse for the echo to appear, thus $\tau_3 \geqslant 0$. When the ratio of τ_1 and τ_2 is set to 1:3, all echoes are separated by τ_1. In the table above, the phase index is the ratio of τ_3/τ_1 for each coherence pathway.

Different coherence pathways create different spatial phase modulation and they yield echo signals at different times, completely separable. As a result, in one scan of the sequence, 5 different modulations can be measured. Thus, we name this class of sequences multiple modulation multiple echoes (MMME), pronounced M-M-Me.

For each coherence pathway Q, molecular diffusion causes a reduction of the signal amplitude by an exponential factor, i.e., from Eq. (13)

$$B_Q = \exp(-b_Q D\gamma^2 g^2 \tau^3). \tag{17}$$

The diffusion number b_Q can be calculated for all coherence pathways and the results for the sequence with the optimal τ ratio are listed above.

It is straightforward to calculate the relaxation effect due to T_1 and T_2 using two numerical parameters, c_{1Q} and c_{2Q}

$$C_Q = \exp\left(-c_{1Q}\frac{\tau_1}{T_1} - c_{2Q}\frac{\tau_1}{T_2}\right). \tag{18}$$

The resulting c_{1Q} and c_{2Q} are listed in the table above.

The above example of 3-pulse sequence can be extended to a general methodology with N pulses, called MMMEN. We have derived that for N pulses

$$\alpha_1\text{–}\tau_1\text{–}\alpha_2\text{–}\tau_2\text{–}\cdots\alpha_N\text{–acquisition}, \tag{19}$$

a total of

$$\frac{3^{(N-1)} - 1}{2} + 1$$

coherence pathways generate observable signals [17]. Each coherence pathway may provide a different modulation (k). In order for the echoes to appear at well separated times during acquisition, one can set the time periods (τ_i) to be powers of 3, for example

$$\tau_i = 3^{i-1}\tau_1. \tag{20}$$

Different permutations of the time periods τ_i will result in a different diffusion and relaxation effects for each coherence pathway, thus offer a mechanism for optimization. For example, with four pulses (MMME4), 14 signals can be recorded, providing 14 different modulations. The FID signal is obtained right after the last pulse due to the coherence pathways such as (0,0,0,0,−1). b_Q was calculated for MMME4 used for the comparison between the theoretical and experimental results in the later section.

This is one of the unique advantages of the MMME technique that the number of modulations is exponential with respect to the number (N) of RF pulses.

The idea of MMME is completely compatible with the use of pulsed field gradient during the precession (τ_i) periods. Similar RF sequences were reported to combine with pulsed field gradients to perform low-resolution imaging experiments [7,8]. The MMME pulses are not limited to the small tipping angles. Also, the tipping angles of all pulses may or may not be equal. It is possible to optimize the tipping angles to enhance or suppress specific coherence pathways and thus the corresponding echoes.

2.4. Recovery due to T_1 relaxation during the sequence

When spin relaxation (both T_1 and T_2) are significant over the time scale of the τ's, the signal from each coherence pathway will be attenuated by an exponential factor dependent on the values of T_1 and T_2. This effect is characterized by the C_Q factor. In addition, T_1 relaxation

will cause recovery of the z-magnetization after each pulse. This z-magnetization may then be rotated and refocused by the subsequent pulses and produce signals. In addition to the N-pulse coherence pathways discussed above, this effect increases the contributing coherence pathways to include those produced by $N-k$ pulses and $k=1,2,\ldots,N-1$. If M^N is used to denote the entire class of coherence pathways for N pulses, the full signal has to include contributions from M^{N-k}

$$M = M^N + \sum_{k=1}^{N-1}[1-\exp(-\tau_k/T_1)]M^{N-k}. \tag{21}$$

Since the phases of echoes due to M^{N-k} will be identical with those of the similar coherence pathways from M^N, these echoes will overlap. Furthermore, the echo shapes can be different, since the coherence pathways are different, i.e. (0,0,1,−1) and (0,1,−1). These effects may complicate the quantitative analysis of the results. On the other hand, the number of echoes affected by this effect is only about 1/3 of the total number of echoes. The experimental results reported in later sections were obtained using a tap-water sample with T_1 of about 3 s and the relaxation effects are much weaker than that due to diffusion and thus ignored.

3. Echo amplitude and shapes

3.1. Hard pulses

It is simpler to illustrate the echo train of MMME sequences by using hard RF pulses. The condition of hard RF pulses can be achieved by using pulsed gradients. For example, the field gradient is turned off before applying RF pulses and turned on afterwards. The effects of the hard pulses are treated by only considering the on-resonance matrix, $\mathbf{R}$, for the rotation of the magnetization vector $\mathbf{M}=(M_+,M_-,M_0)$

$$\mathbf{M}(t_p)=\mathbf{R}(\alpha)\mathbf{M}(0)$$

and

$$\mathbf{R}(\alpha)=\begin{pmatrix} \frac{1+\cos\alpha}{2} & \frac{1-\cos\alpha}{2}e^{2i\phi} & -i\frac{\sin\alpha}{\sqrt{2}}e^{i\phi} \\ \frac{1-\cos\alpha}{2}e^{-2i\phi} & \frac{1+\cos\alpha}{2} & i\frac{\sin\alpha}{\sqrt{2}}e^{-i\phi} \\ -i\frac{\sin\alpha}{\sqrt{2}}e^{-i\phi} & i\frac{\sin\alpha}{\sqrt{2}}e^{i\phi} & \cos\alpha \end{pmatrix}, \tag{22}$$

where α is the on-resonance tipping angle of the pulse of length t_p. This case of on-resonance rotations has been discussed previously [7,8] for imaging experiments. We will analyze the tipping-angle dependence in detail and derive a procedure to obtain the optimal angles.

For a hard-pulse MMME4 sequence, spin echoes can form for 13 coherence pathways and an FID is measurable for one coherence pathway. The signals and the corresponding coherence pathways are given as:

$$(0,0,0,0,-): I_0 = \frac{i}{\sqrt{2}}\cos\alpha_1\cos\alpha_2\cos\alpha_3\sin\alpha_4 e^{-\phi_4}, \tag{23}$$

$$(0,+,0,0,-): I_1 = \frac{-i}{2\sqrt{2}}\sin\alpha_1\sin\alpha_2\cos\alpha_3\sin\alpha_4 e^{i(\phi_1-\phi_2-\phi_4)}, \tag{24}$$

$$(0,-,+,0,-): I_2 = \frac{i}{4\sqrt{2}}\sin\alpha_1(1-\cos\alpha_2)\times\sin\alpha_3\sin\alpha_4\times e^{-i(-\phi_1+2\phi_2-\phi_3-\phi_4)}, \tag{25}$$

$$(0,0,+,0,-): I_3 = \frac{-i}{2\sqrt{2}}\cos\alpha_1\sin\alpha_2\sin\alpha_3\sin\alpha_4\times e^{-i(\phi_2-\phi_3-\phi_4)}, \tag{26}$$

$$(0,+,+,0,-): I_4 = \frac{-i}{4\sqrt{2}}\sin\alpha_1(1+\cos\alpha_2)\sin\alpha_3\sin\alpha_4\times e^{-i(\phi_1-\phi_3-\phi_4)}, \tag{27}$$

$$(0,-,-,+,-): I_5 = \frac{i}{8\sqrt{2}}\sin\alpha_1(1+\cos\alpha_2)(1-\cos\alpha_3)\times(1-\cos\alpha_4)\times e^{-i(-\phi_1+2\phi_3-2\phi_4)}, \tag{28}$$

$$(0,0,-,+,-): I_6 = \frac{i}{4\sqrt{2}}\cos\alpha_1\sin\alpha_2(1-\cos\alpha_3)(1-\cos\alpha_4)\times e^{-i(-\phi_2+2\phi_3-2\phi_4)}, \tag{29}$$

$$(0,+,-,+,-): I_7 = \frac{-i}{8\sqrt{2}}\sin\alpha_1(1-\cos\alpha_2)\times(1-\cos\alpha_3)(1-\cos\alpha_4)\times e^{-i(\phi_1-\phi_2+2\phi_3-2\phi_4)}, \tag{30}$$

$$(0,-,0,+,-): I_8 = \frac{i}{4\sqrt{2}}\sin\alpha_1\sin\alpha_2\sin\alpha_3\times(1-\cos\alpha_4)\times e^{-i(\phi_1+\phi_2+\phi_3-2\phi_4)}, \tag{31}$$

$$(0,0,0,+,-): I_9 = \frac{-i}{2\sqrt{2}}\cos\alpha_1\cos\alpha_2\sin\alpha_3\times(1-\cos\alpha_4)\times e^{-i(\phi_3-2\phi_4)}, \tag{32}$$

$$(0,+,0,+,-): I_{10} = \frac{i}{4\sqrt{2}}\sin\alpha_1\sin\alpha_2\sin\alpha_3\times(1-\cos\alpha_4)\times e^{-i(\phi_1-\phi_2+\phi_3-2\phi_4)}, \tag{33}$$

$$(0,-,+,+,-): I_{11} = \frac{i}{8\sqrt{2}}\sin\alpha_1(1-\cos\alpha_2)(1+\cos\alpha_3)\times(1-\cos\alpha_4)\times e^{-i(\phi_1-2\phi_2-2\phi_4)}, \tag{34}$$

$$(0,0,+,+,-): I_{12} = \frac{-\mathrm{i}}{4\sqrt{2}} \cos\alpha_1 \sin\alpha_2 (1+\cos\alpha_3) \times (1-\cos\alpha_4) \times \mathrm{e}^{-\mathrm{i}(\phi_2 - 2\phi_4)}, \quad (35)$$

$$(0,+,+,+,-): I_{13} = \frac{-\mathrm{i}}{8\sqrt{2}} \sin\alpha_1 (1+\cos\alpha_2)(1+\cos\alpha_3) \times (1-\cos\alpha_4) \times \mathrm{e}^{-\mathrm{i}(\phi_1 - 2\phi_4)}. \quad (36)$$

Here, I_0 gives an FID and each of $I_n (n = 1, 2, \ldots, 13)$ gives an echo. When $\tau_1 = \tau_2/3 = \tau_3/9 = \tau$ as discussed earlier, the 13 echoes are separated from each other and appear at $t = n\tau$. Most other NMR methods for diffusion often single out one coherence pathway by exploiting the signal dependence on the phase of the RF pulses, ϕ_1, ϕ_2, ϕ_3, and ϕ_4. The MMME method generates echoes at different times and hence, all echoes can be obtained individually in a single scan. Thus, no phase cycling is needed and all phases may be set to zero.

3.2. Optimization of pulse angles

The above Eqs. (23)–(36) show that it is impossible to find a set of flip angles to equalize the magnitude of all echoes. This can be understood by observing the four different flip-angle dependences among the 13 MMME echoes for all RF pulses except the first and the last. On the other hand, the magnitude difference among the MMME echoes can be minimized. For the first RF pulse, the flip-angle dependence is either $\sin\alpha_1/\sqrt{2}$ (when rotating $q_0 = 0$ to $q_1 = \pm 1$) or $\cos\alpha_1$ (when rotating $q_0 = 0$ to $q_1 = 0$). These two terms are equal when $\alpha_1 = \arcsin\sqrt{2/3}$, $\sin\alpha_1/\sqrt{2} = \cos\alpha_1 = 1/\sqrt{3}$. For the last pulse, the flip-angle dependence is either $\sin\alpha_4/\sqrt{2}$ or $(1-\cos\alpha_4)/2$. Similarly, they are equal when $\alpha_4 = \arccos(-1/3)$.

All other RF pulses involve four types of the flip-angle dependence, i.e., $\sin\alpha/\sqrt{2}, \cos\alpha, (1+\cos\alpha)/2$, and $(1-\cos\alpha)/2$. The minimum spread of the signals is achieved at $\alpha = \arccos(1/3)$ when

$$\frac{1+\cos\alpha}{1-\cos\alpha} = \frac{\sin\alpha}{\sqrt{2}\cos\alpha}$$

and also for $\alpha = \arccos(-1/3)$ when

$$\frac{1-\cos\alpha}{1+\cos\alpha} = \frac{\sin\alpha}{\sqrt{2}\cos\alpha}.$$

For both cases, $\sin\alpha/\sqrt{2} = 2/3$, $|\cos\alpha| = 1/3$ and $|1 \pm \cos\alpha|/2$ is either 1/3 or 2/3. This optimum can be easily seen from Fig. 1, where the four types of flip-angle dependence are shown.

From Eqs. (23)–(36), the signal amplitude is dependent on the product of the factors of the first and last pulses, and the two angular factors associated with the two pulses α_2 and α_3. Since each of the two angular factors for α_2 and α_3 consist of all four types, the product of the two minima (or the maxima) will determine the minimum (or the maximum) of the final signal. As a result, the optimal tipping angles are: $\alpha_1 = 54.74°, \alpha_2 = \alpha_3 = 70.53°$, and $\alpha_4 = 109.47°$ and the amplitudes of the 13 echoes become: $\mathrm{i}\sqrt{3}/81(-4, 4, -8, -8, 4, 4, -2, 8, -4, 8, 4, -8, -8)$.

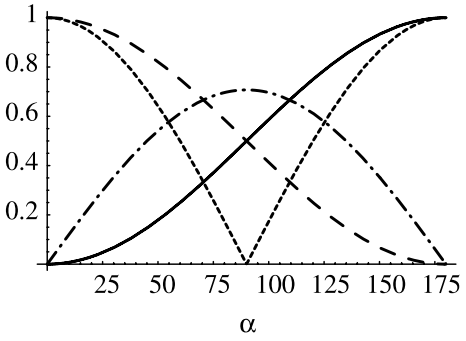

Fig. 1. Four types of angular dependence are shown: $\sin\alpha/\sqrt{2}$ (dash-dot line), $|\cos\alpha|$ (short dashed line), $(1+\cos\alpha)/2$ (long dashed line), and $(1-\cos\alpha)/2$ (solid). At $\alpha = 70.53°$ ($\cos\alpha = 1/3$), the spread of the four factors is minimum.

Two interesting features are of note. First, the sum of the magnitude of the 13 echoes is $74\sqrt{3}/81$, which is 2.24 times the magnitude of a Hahn echo (generated by the 90°–180° sequence) as $\sin(\pi/2)(1-\cos\pi)/2\sqrt{2} = 1/\sqrt{2}$. The magnitude of the six largest echoes is about one quarter of that of the Hahn echo. Except for the 7th echo the magnitude difference among all echoes is only a factor of 2.

The above conclusions can be generalized to a MMME sequence with N RF pulses. When the flip angles are set as: $\alpha_1 = 54.74°, \alpha_2 = \alpha_3 = \cdots = \alpha_{N-1} = 70.53°$, and $\alpha_N = 109.47°$, then the weakest echo is the number $(3^{N-1}+1)/4$ echo for even N's or the number $(3^{N-1}-1)/4$ echo for odd N's. Except for this echo, the magnitude difference among all echoes is only a factor of 2^{N-3}.

3.3. Soft pulses

For experiments in constant field gradient and extended sample size along the gradient direction, it is often that the off-resonance signals cannot be neglected. In this case, each pulse is slice-selective and the frequency dependence needs to be included explicitly to understand the spin dynamics to evaluate the echo amplitude and shapes.

Eq. (11) shows that A_Q is dependent on the frequency offset, thus it determines the frequency spectrum and the echo shape of each coherence pathway. The spectra and time domain echo shapes can be evaluated numerically using Eq. (11) provided that the spatial RF and magnetic field profiles are known. We have assumed a constant RF amplitude and field gradient, thus the spectrum of an MMME4 echo is given by

$$\Lambda_1\Lambda_2\Lambda_3\Lambda_4 \tag{37}$$

and

$$\Lambda_i = R_{q_{i-1}q_i}(\Delta\omega, \omega_1, t_{pi}, \phi), \tag{38}$$

where t_{pi} is the length of the ith pulse. We have evaluated numerically the frequency spectra of the MMME4 sequence with $\alpha_1 = \alpha_2 = \alpha_3 = 90°$ and $\alpha_4 = 180°$ and the phase of all pulses was set to zero. The spectrum for each coherence pathway and echo is shown in Fig. 2. The time-domain echo shapes, Fig. 3, were obtained by the Inverse Fourier transformation of the corresponding spectrum.

An MMME4 experiment on a tap water sample was performed and the resulting echoes are shown in Fig. 4. The echo shapes of the theoretical calculation clearly reproduce the experimental results for each echo. In particular, the maximum of many echoes occurs away from the echo center which is defined by $n\tau_1$ after the last pulse. This is due to the spatial modulation of the spectrum. To compare quantitatively the theoretical evaluation and the experimental results, we define the signal amplitude for the nth echo $I_n(t)$ by the following formula

$$S_n = \sqrt{\int \mathrm{d}t I_n(t) I_n^*(t)}, \tag{39}$$

which is essentially the signal power. Certainly, other definitions can be used such as the matched filter. In the last panel of Fig. 4, the amplitudes for all 13 echoes are compared between theoretical and experimental results showing a very good agreement.

3.4. Methods using two scans

One of the possible ways to use MMME sequences to determine diffusion is by repeating the sequence, for instance, MMME4, with two sets of τ_i with $\tau_1 = \tau$ and τ', while keeping the ratio the same. Then, the shapes of the corresponding echoes will be identical and their amplitude ratio can be found to be

$$\frac{S_Q(\tau)}{S_Q(\tau')} = \exp[-b_Q D\gamma^2 g^2(\tau^3 - \tau'^3)]. \tag{40}$$

Each pair of the echoes will give one data point for the diffusion decay and a total of 13 data points can be obtained by the two acquisitions, as shown in Fig. 5.

If measurement speed is of concern, the following method can be used to calibrate the echo shapes using a standard sample of small or known diffusion constant. The first experiment can be performed with the standard sample using the same sequence, possibly with a small τ to minimize the diffusion effects. From this experiment, the echo shapes without diffusion decay can be obtained. Then, one scan on other samples with a selected τ is sufficient for obtaining data of multiple k.

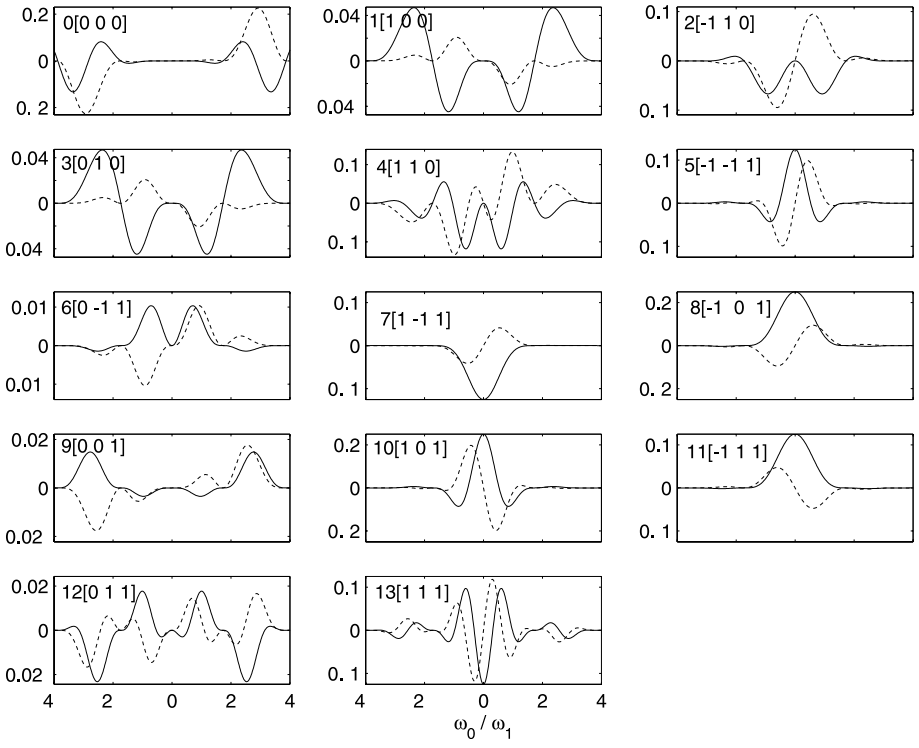

Fig. 2. Theoretical frequency spectra (solid lines for the imaginary part and dashed lines for the real part) for each coherence pathway of MMME4 (90°–90°–90°–180°). The labels inside the echo boxes are echo numbers, coherence pathways (inside the bracket parentheses). The first box shows the FID signal right after the last pulse ($n = 0$).

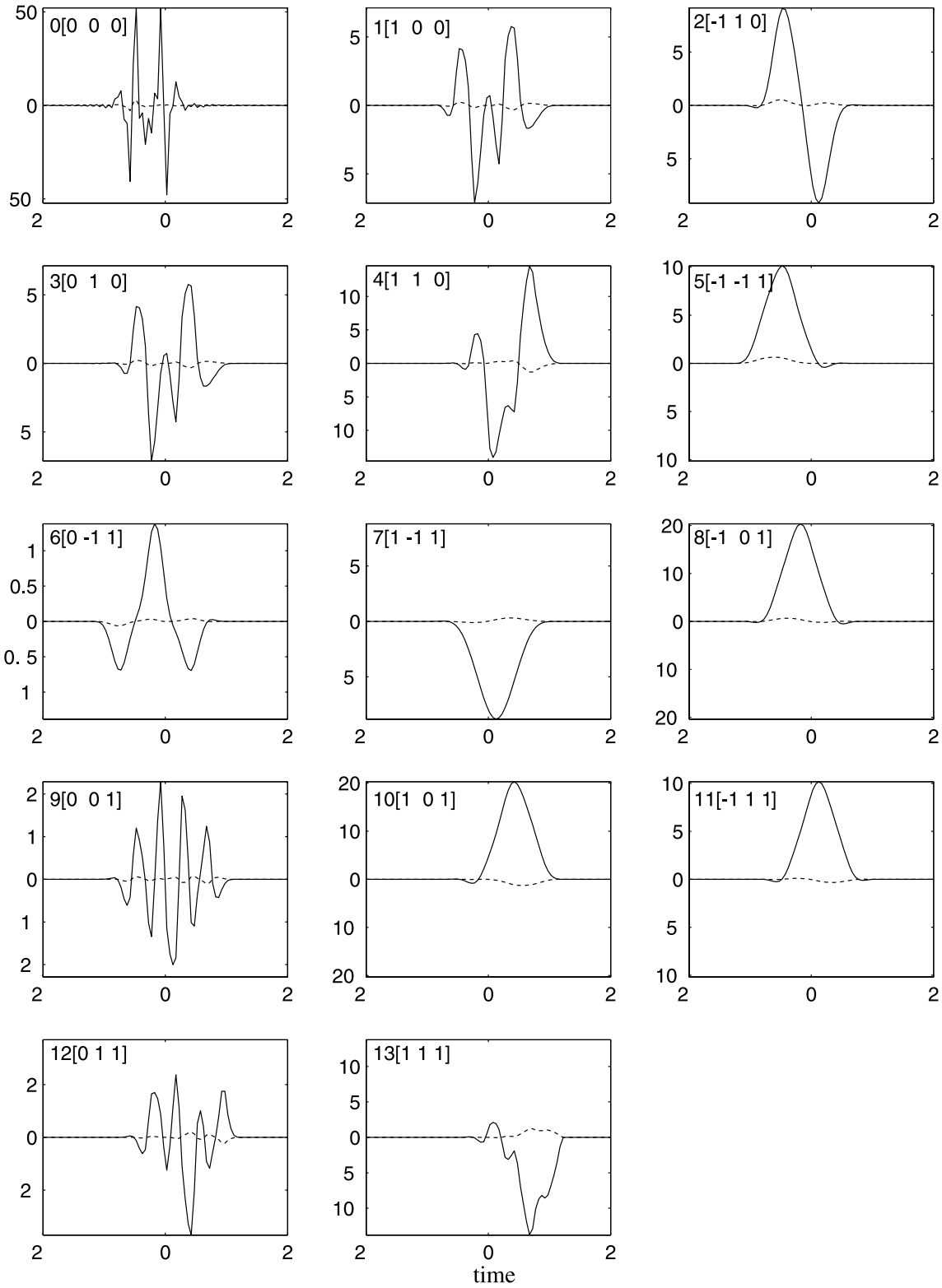

Fig. 3. Theoretical echo shapes for MMME4 (90°–90°–90°–180°) for each coherence pathway, solid lines for the imaginary part and dashed lines for the real part. The horizontal axis is time in units of the π pulse length. The labels inside the echo boxes are echo numbers and coherence pathways (inside the bracket parentheses). The first box shows the FID signal right after the last pulse. The center time of the echo, $t = n\tau_1$, corresponds to the middle of the box where the time is labeled zero. Note that the maximum of many echoes does not occur at the center.

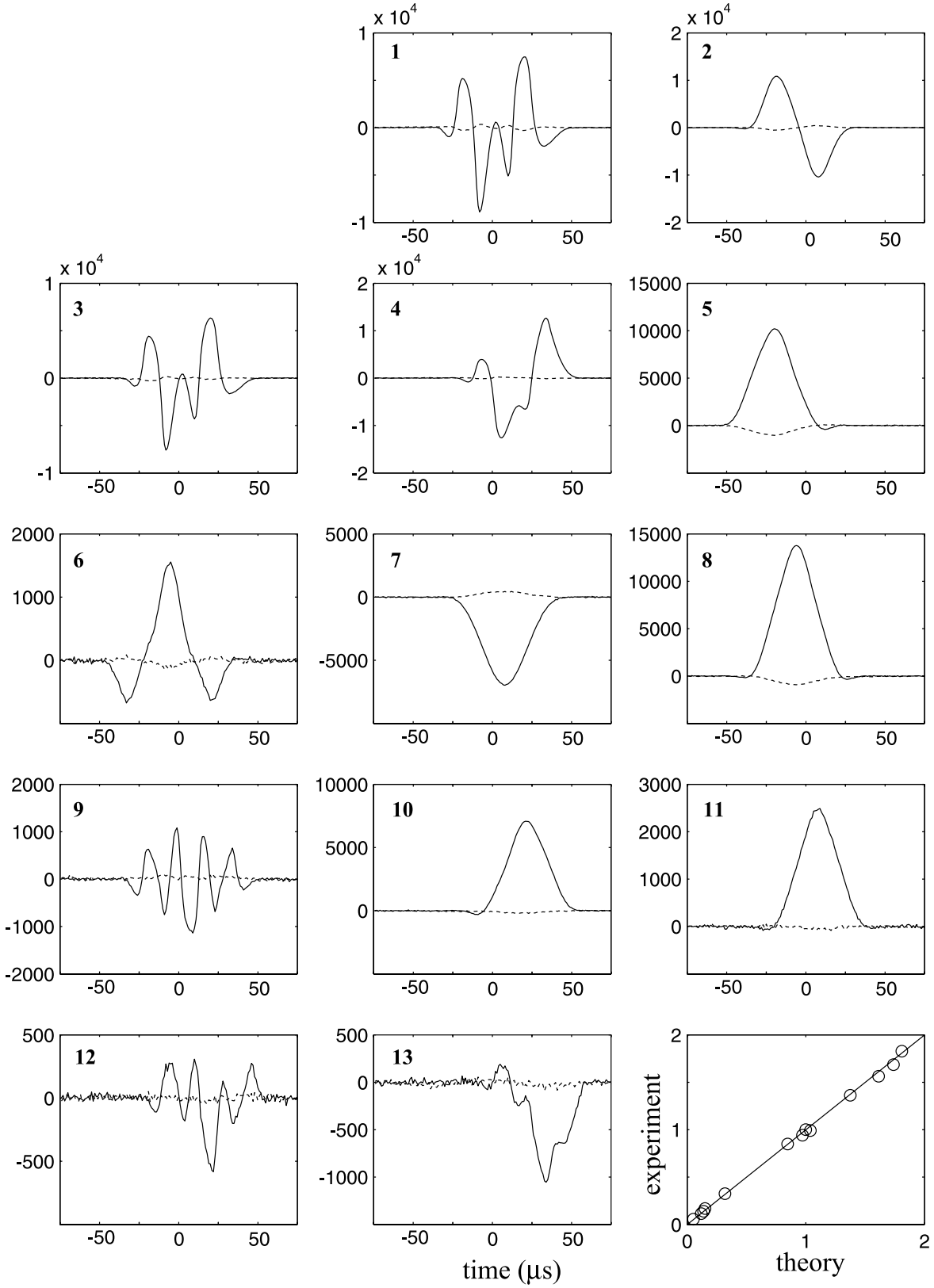

Fig. 4. Experimental echo shapes (solid lines for the imaginary part and dashed lines for the real part) for MMME4 obtained for bulk water at 2 T field with 6 G/cm gradient. Echo numbers (listed in each box) are ordered in the same fashion as in Fig. 3. The τ ratio was 3 and $\tau_1 = 1.5$ ms. The first three pulses were 90° pulses of 115 μs duration and the fourth one a 180° pulse 230 μs long. The time zero corresponds to the center of each echo. Note that the maximum of the echoes often occurs away from the center position. The sample was a cylinder, 2 cm diameter and approximately 8 cm long along the gradient direction. The last figure shows the theoretical amplitude vs the experimental one.

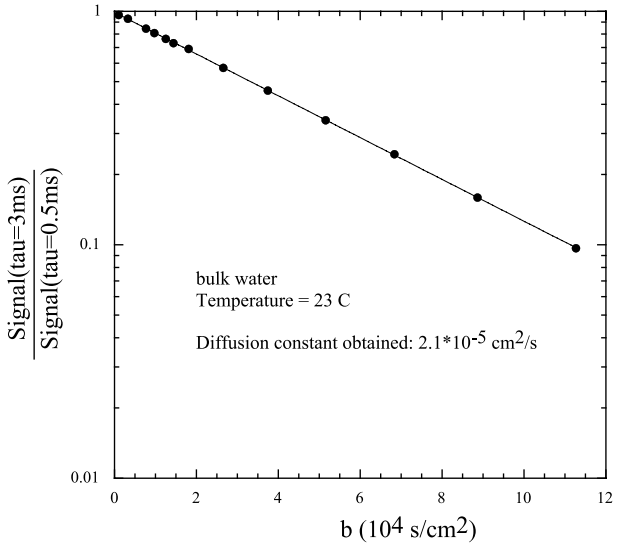

Fig. 5. MMME4 result for measuring the diffusion constant in bulk water. MMME4 echoes were obtained with $\tau = 0.5$ and $\tau' = 3$ ms and signal amplitude for echoes was determined using Eq. (39). The ratio of the corresponding echo signals is shown for all 13 echoes as a function of the $b \equiv \gamma^2 g^2 b_Q(\tau'^3 - \tau^3)$. The single exponential decay of the data points is consistent with the single diffusion constant of water. The slope of the decay determines the diffusion constant to be 2.1×10^{-5} cm^2/s.

3.5. Methods using one scan

3.5.1. Fringe field or constant gradient for large uniform sample

In the presence of a constant field gradient, all RF pulses are essentially slice-selective pulses that excite only a region of sample, where the resonance frequencies are close to the RF irradiation frequency. If the sample is significantly larger than such volume and the RF field is spatially constant or known, one can calculate the echo signals and shapes rigorously. This is the case shown in Figs. 3 and 4. In this case, one scan of the MMME sequence will be sufficient to determine the diffusion coefficient.

3.5.2. Arbitrary sample size

On the other hand, if the sample size is comparable or smaller than the slice thickness, or the spatial RF profile is unknown, one may not be able to calculate the signal shapes for all echoes. In this case, one can show that some of the coherence pathways produce identical echo shapes. For MMME4, the following pairs of echoes are closely related: echoes 1 and 3 have identical shape and amplitude, echoes 5 and 10 have identical shape and their amplitude ratio is 1/2, and echoes 8 and 11 have identical shape and their amplitude ratio is 1/2. Thus, from measurement of 13 echoes, there are in total 10 unknowns for the amplitudes, one unknown for the diffusion constant, D. As a result, D can be determined from one scan of MMME4.

Furthermore, if T_1 and T_2 relaxation decays are not negligible during τ_i's, these relaxation decay factors can be calculated for each coherence pathway [12]. With 13 data points and 13 unknowns (10 amplitudes, D, T_1, and T_2), D, T_1, and T_2 can all be obtained in one scan.

In addition, MMME5 will yield 40 echoes and may provide even better measurement of D, T_1, and T_2 in one scan.

4. Stimulated MMME: MMME as a unit in stimulated-echo-type sequence

4.1. General description

The pulsed-field gradient stimulated echo technique is commonly used for measuring diffusion. In a typical experiment, the spin magnetization is rotated into the transverse plane by a 90° pulse and it then precesses in a field gradient. A second 90° pulse turns the spatially modulated magnetization back to the z-axis. After a time period to allow diffusion, a third 90° pulse rotates spins into the transverse plane to form a stimulated echo. Between the first and second pulses normally only one coherence pathway is selected and hence one modulation is utilized. The DIFFTRAIN technique [18,19] accelerates the diffusion measurement by observing the decay of the modulated magnetization at several diffusion times. Peled et al. [11] further extended the method by introducing multiple modulation in the initial encoding period and observing the signal decay due to diffusion at several diffusion times. However, the multiple modulations were obtained by using small tipping angle pulses. We will compare different methods in details later in the paper.

The MMME idea can be incorporated into the stimulated echo sequence to create multiple modulations within one scan to retrieve diffusion information from several coherence pathways. For example, MMME can be used in the initial modulation period, followed by a long waiting period, then a detection period

$$\mathrm{MMME} - \Delta_1 - \theta_1 - \Delta_2 - \theta_2 - \cdots \tag{41}$$

Acquisitions of echo signals can be made during the multiple Δ periods. Here, the MMME segment is used as the encoding unit to create multiple modulations in contrast to the conventional stimulated echo with one modulation. In the first acquisition period after θ_1, two groups of echoes will be observed. The first group appears after the θ_1 pulse in the order of the same MMME sequence, for instance, the 13 echoes of MMME4. The coherence pathways of these echoes follow the form of $(Q_{\mathrm{MMME}}, 0, -1)$, where Q_{MMME} is the corresponding coherence pathway of the MMME sequence, the 0 and 1 are the coherence states during Δ_1 and Δ_2. In sequences

with additional θ pulses, similar echoes appear after each θ pulse and their coherence pathways are of the form $(Q_{\mathrm{MMME}}, 0, \ldots, 0, -1)$ where $q = 0$ occurs during all of the intervening Δ periods. Such coherence pathways are very similar to that of the stimulated echo, thus we call the corresponding echoes stimulated multiple echoes (STME). In the rest of the paper, we will label the echoes after the ith θ pulse $E(i,n)$, where the index n refers to the echo number within the group. In this notation, $E(0,n)$ denotes the echoes after the MMME segment.

Starting from a time Δ_1 after the θ_1 pulse, another group of echoes appears whose coherence pathways are of the form $(Q_{\mathrm{MMME}}, +1, -1)$. This second group may often be unwanted and can be removed by phase cycling or additional field gradient pulses during the Δ_1 period. With further θ pulses, more echoes with coherence pathways other than STME will appear. They can be most effectively canceled by field gradient pulses during the multiple Δ periods.

From Eq. (13), the diffusion decay factor for each STME echo can be obtained by the following argument. For the nth echo after the θ_i pulse, the modulation before the θ pulse is k_n. Thus, from Eq. (13)

$$\begin{aligned}\log\left[B_Q(i,n)\right] &= -D\int \mathrm{d}t\, k(t)^2 \\ &= \log\left[B_Q(0,n)\right] - Dk_n^2(\Delta_1 + \Delta_2 + \cdots + \Delta_i),\end{aligned} \tag{42}$$

where $B_Q(0,n)$ is the corresponding factor for the respective MMME echo. The second term indicates that the additional decay of STME is proportional to the square of the modulation (k), completely analogous to the decay of the conventional stimulated echo due to diffusion. The benefit of STME is that multiple modulation can be obtained in one scan of the sequence.

From Eq. (11), the RF pulses affect the echo amplitude through the multiplicative factor (A_Q) which is the product of RF rotation matrix element Λ for all the α pulses in the MMME segment and all the θ pulses afterwards. For a known RF profile and sample geometry, A_Q can be evaluated for all echoes. It is also useful to compare the A_Q factors for different groups of STME, for example, STME after the ith and jth θ pulses.

$$\frac{A_Q(j,n)}{A_Q(i,n)} = \frac{\Lambda_{00}(i)\Lambda_{0-}(j)}{\Lambda_{0-}(i)}\prod_{l=i+1}^{l=j-1}\Lambda_{0,0}(l), \tag{43}$$

where the parameters for Λ: $\omega_{1l}, \omega_{1l}, t_{pl}, \phi_l$ are replaced by an index l of the θ pulse, for clarity. For the on-resonance signal, $\delta\omega = 0$ and the above formula can be simplified to $\cot\theta_i \cos\theta_{i+1}\cdots\cos\theta_{j-1}\sin\theta_j$. It is important to note that this factor is the same for all echoes and thus the diffusion decay factor B_Q can be obtained by the ratio of two sets of STME.

4.2. Experimental results with stimulated-MMME

We conducted a measurement by applying the stimulated-MMME4 sequence

$$(\alpha_1\text{–}\tau\text{–}\alpha_2\text{–}3\tau\text{–}\alpha_3\text{–}9\tau\text{–}\alpha_4)\text{–}\Delta_1\text{–}\theta_1\text{–}\Delta_2\text{–}\theta_2\text{–}, \tag{44}$$

where $\tau = 1\,\mathrm{ms}$, $\Delta_1 = 45\,\mathrm{ms}$, and $\Delta_2 = 90\,\mathrm{ms}$. Signals of STME were acquired during each Δ period. Thirteen coherence pathways generated by the MMME4 segment led to observable echoes with the corresponding modulations $\gamma g\tau$, $2\gamma g\tau$, …,$13\gamma g\tau$ for the respective echoes. The magnitude ratios between the corresponding echoes of the first and second STME trains are shown in Fig. 6 and they determine correctly the water diffusion constant of $2.18\times10^{-9}\,\mathrm{m}^2/\mathrm{s}$.

We can also compare the MMME signals with the STME signals, at least for the on-resonance case (either obtained by integration of the echo signal or by using strong RF pulses). For the first four echoes of MMME4 appearing right after α_4, the matrix element associated with α_4 is $\Lambda_4 = \sin\alpha_4/\sqrt{2}$. For the last nine echoes, it is $(1-\cos\alpha_4)/2$. Similarly, for the first four echoes of the first STME train, $\Lambda_4 = \cos\alpha_4$ and the last 9 echoes, $\sin\alpha_4/\sqrt{2}$. Therefore, the ratio $A_Q(1,n)/A_Q(0,n)$ is $\cot\alpha_4\sin\theta_1$ for $n = 1$–4, and $\sin\alpha_4\sin\theta_1/(1-\cos\alpha_4)$ for $n = 5$–13. Therefore, these two ratios can also be used to obtain the diffusion constant. Indeed, both relationships are well reproduced in Fig. 6 and the resulting diffusion constant is in agreement with previous data.

Even though the above discussion is focused on the determination of the diffusion constant, it can also be used to obtain the diffusion propagator [5] in one scan. Furthermore, by using multiple θ pulses, the diffusion constant and the diffusion propagator at different times can be obtained in one scan.

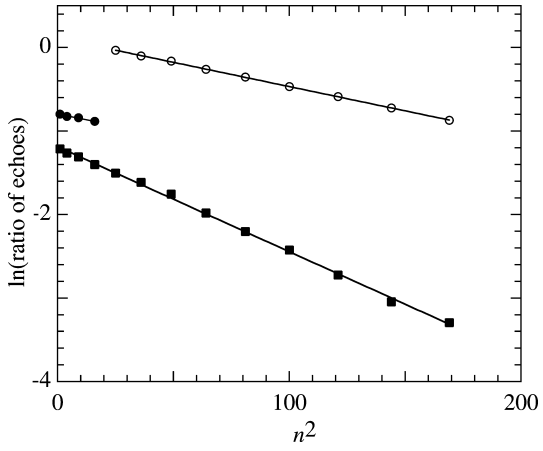

Fig. 6. Decay of the ratio of the integrated echo signals as a function of the square of echo number n^2. The solid squares are the ratio of the second and first STME trains $\ln[E(2,n)/E(1,n)]$, solid circles are that of the first STME train and the MMME train, $\ln[E(1,n)/E(0,n)]$ with $n = 1$–4, and the open circles are those with $n = 5$–13.

5. Previous one-shot diffusion measurement techniques

Two previous papers [10,11] are most relevant to the current technique. In these two papers, small tipping angle (often less than 1°) pulses were mandatory to create multiple magnetization modulation (called gratings in some literature) and multiple echoes were detected in a fashion similar to spin-echo [10] and stimulated echo [11]. The use of the train of small tipping angle pulses is often called BURST or DUFIS. In these schemes, one pulse can only create one modulation (or echo) of substantial amplitude. Thus, both of these previous techniques are inefficient in two ways. First, to create N echoes, N excitation pulses will be used, while in the MMME method, only about $\log_3(2N+1)$ pulses will be needed. Second, both previous techniques can only use a small portion of the total signal and a significant fraction of the magnetization is still left along the z-axis. In the current method, essentially all the magnetization can be utilized for creating signals.

We will analyze the DUFIS sequence for diffusion measurement in some detail in order to have a direct comparison with the MMME sequence. The DUFIS sequence consists of a series of small tipping angle pulses (α) equally spaced in time before a π pulse,

$$[\alpha\text{–}\tau\text{–}]_N\text{–}\pi\text{–acquisition} \tag{45}$$

under a constant field gradient g. The desirable coherence pathways giving rise to the echoes equally spaced by τ after the detections are:

$$Q_{\mathrm{DUFIS}} = \underbrace{0\cdots0}_{k}\,\underbrace{1\cdots1}_{N-k}, -1, \text{and } k = 0,\ldots,N-1. \tag{46}$$

Strictly speaking, all these coherence pathways will result in different signals since Qs are not the same. It was realized that at small α, the differences in the echo shapes are small enough so that the diffusion effect can be determined assuming the constant echo shape. In Fig. 7, the spectra of eight echoes in a DUFIS sequence with $N = 8$ are shown to progress from the relatively uniform shape at $\alpha = 1°$ to dramatically difference at $\alpha = 5°$.

In addition to the shape changes among the DUFIS echoes, many coherence pathways contribute to the echoes except the last one—there is only one coherence pathway to create the last echo. For example, for $N = 8$, there are 1015 and 784 additional pathways contributing to the first and second echoes. The amplitudes of these pathways increase significantly as the tipping angle of α pulses increases. Fig. 7 compares the sums of all DUFIS echoes and all other pathways as a function of α. It appears that the non-DUFIS pathways contribute to about 10% of the echo signal even at $\alpha = 1°$, and much more as α increases. The optimized sequence (OUFIS) [20] reduces the non-DUFIS pathways by approximately a factor of 3 (Fig. 7). Thus, the simple interpretation of the echo amplitude assuming constant shape can be inaccurate even at very small α.

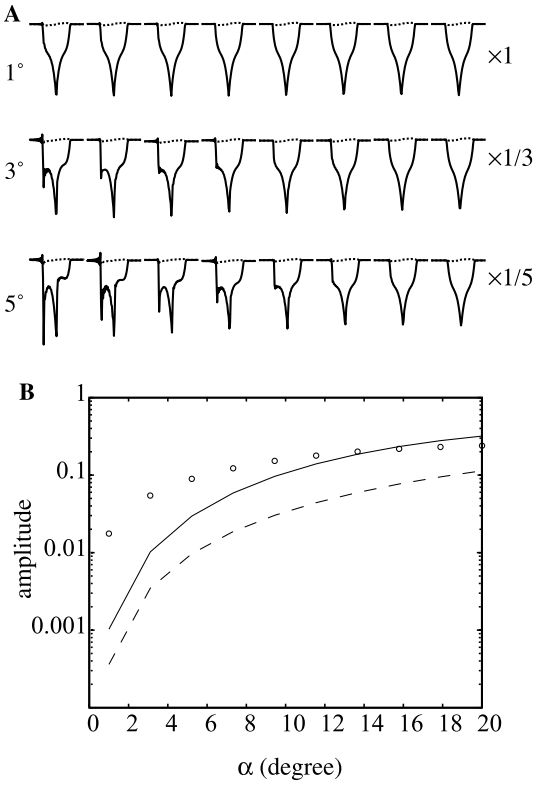

Fig. 7. (A) Theoretical echo shapes (real part, dotted lines; imaginary part, solid lines) from a DUFIS 8 sequence for $\alpha = 1°, 3°$, and 5°. The echoes at larger tipping angles are distorted compared to those at $\alpha = 1°$. A time period of four π pulse length around the echo center is shown for each echo. The amplitude of the echoes are scaled by the numerical factors shown on the side. (B) Plot of the average of DUFIS echo amplitude (circles), normalized to that of a Hahn echo, as a function of α. Comparison is made with the sum of other pathways in a DUFIS sequence (solid line) and OUFIS (dashed line).

The non-DUFIS coherence pathways will have a diffusion-induced signal decay that is different from the DUFIS pathways and in general different for each pathway. Thus, the presence of the large number of pathways in the DUFIS echoes makes it difficult to analyze the diffusion effects at α larger than 1°. As a result, previous reports of DUFIS experiments had limited the tipping angles of the excitation pulses. This requirement limits the detected signals to only a small fraction of the total available magnetization of the sample.

Compared to the DUFIS method, our present approach (MMME) has the following advantages that:

- there are only a few pulses needed to produce many echoes, resulting potentially in less RF deposition in the sample,
- one echo contains signal from only one coherence pathway, thus the diffusion effect is well defined,
- the pulses are not limited to small tipping angles, e.g., 90°–90°–90°–$\cdots$–180°,

- the echo signals represent a substantial portion of the available magnetization of the sample.

Discussion of the MMME technique will not be complete without exploring its limitation.

- Short T_2: in any diffusion experiment using phase encoding, there is always a trade-off between T_2 and the available gradient strength. This is simply because T_2 decay occurs during gradient encoding and decoding. The minimum encoding time is determined by the maximum gradient available and the range of diffusion constant to be detected. There is no fundamental difference between MMME and the stimulated echo or DIFFTRAIN.
- S/N: each MMME echo is weaker than the stimulated echo. However, the total signal summed over all echoes is larger than the stimulated echo, e.g., more than four times for MMME4. Thus, the ratio of total signal and total noise is close to that of the stimulated echo. For example, the error of diffusion constant is determined more by the total signal-to-noise ratio. In this regard, MMME and DIFFTRAIN exhibit similar total S/N.
- Complex relaxation: the relaxation effect is different for different echoes, thus potentially complicates the interpretation. If the relaxation decay is small or the functional form of the decay is known, the relaxation time (T_1 and T_2) can be obtained from the MMME data as discussed previously. If the relaxation is non-exponential and not known, then another reference scan at a different gradient value can be used as a normalization. Similar issue exists for other one-scan methods, such as BURST and DIFFTRAIN.
- Diffusion propagator: the regular MMME (e.g., with time intervals to be 1:3:9, etc.) may not be a good method for propagator measurement due to the lack of well defined diffusion time. On the other hand, Stimulated-MMME can be an excellent method for it by using a diffusion time much longer than the encoding time. In this case, the diffusion time for every echo is essential a constant and the multiple echoes will determine the propagator at multiple k.

6. Conclusions

We present a novel NMR methodology for truly rapid measurement of diffusion properties. This method uses a few RF pulses and static or pulsed field gradient to create and observe multiple coherence pathways. Signals from all coherence pathways are well separated in time, and no phase cycling is needed, thus enabling a truly rapid measurement.

We outline the theoretical treatment of the spin dynamics during the multiple RF pulses and field gradient including the off-resonance effects which is crucial for diffusion and imaging experiments. The theoretical echo shapes and echo decays are found to be consistent with the experimental results. The theoretical framework can be useful to simulate the signals for given RF and sample profiles and to optimize the pulse sequences, i.e., flip angles of the pulses.

The high speed of this method is one of its major advantage that will enable the observation of time-sensitive processes. Its potential applications include fluid characterization, medical MRI and the monitoring of material processing and chemical reactions.

Acknowledgment

The authors thank Dr. D. Madio for comments.

References

[1] E.L. Hahn, Spin echoes, Phys. Rev. 80 (1950) 580.
[2] E.O. Stejskal, J.E. Tanner, Spin diffusion measurements: spin echoes in the presence of a time-dependent field gradient, J. Chem. Phys. 42 (1965) 288.
[3] D.E. Woessner, NMR spin-echo self-diffusion measurements on fluids undergoing restricted diffusion, J. Phys. Chem. 67 (1963) 1365.
[4] P.P. Mitra, P.N. Sen, L.M. Schwartz, P. Le Doussal, Diffusion propagator as a probe of the structure of porous media, Phys. Rev. Lett. 68 (1992) 3555.
[5] J. Kärger, W. Heink, The propagator representation of molecular transport in microporous crystallites, J. Magn. Reson. 51 (1983) 1.
[6] P.T. Callaghan, A. Coy, D. MacGowan, K.J. Packer, F.O. Zelay, Diffraction-like effects in NMR diffusion studies of fluids in porous solids, Nature 351 (1991) 467.
[7] C.J. Counsell, PREVIEW: a new ultrafast imaging sequence requiring minimal gradient switching, Magn. Reson. Imaging 11 (1993) 603.
[8] O. Heid, M. Deimling, W. Huk, QUEST—a quick echo split NMR imaging technique, Magn. Reson. Med. 29 (1993) 280.
[9] I.J. Lowe, R.E. Wysong, DANTE ultrafast imaging sequence (DUFIS), J. Magn. Reson. B 101 (1993) 106.
[10] S.J. Doran, M. Décorps, A robust, single-shot method for measuring diffusion coefficients using the "Burst" sequence, J. Magn. Reson. A 117 (1995) 311.
[11] S. Peled, C.H. Tseng, A.A. Sodickson, R.W. Mair, R.L. Walsworth, D.G. Cory, Single-shot diffusion measurement in laser-polarized gas, J. Magn. Reson. 140 (1999) 320.
[12] M.D. Hürlimann, Diffusion and relaxation effects in general stray field NMR experiments, J. Magn. Reson. 148 (2001) 367.
[13] Y.-Q. Song, Categories of coherence pathways in the CPMG sequence, J. Magn. Reson. 157 (2002) 82.
[14] P.T. Callaghan, Principles of Nuclear Magnetic Resonance Microscopy, Oxford University Press, New York, 1993.
[15] A. Sodickson, D.G. Cory, A generalized k-space formalism for treating the spatial aspects of a variety of NMR experiments, Prog. NMR Spectrosc. 33 (1998) 77.
[16] L.J. Zielinski, P.N. Sen, Restricted diffusion in grossly inhomogeneous fields, J. Magn. Reson. 164 (2003) 145.
[17] R.J. Nelson, Y. Maguire, D.F. Caputo, G. Leu, Y. Kang, M. Pravia, D. Tuch, Y.S. Weinstein, D.G. Cory, Counting echoes:

application of a complete reciprocal-space description of NMR spin dynamics, Concepts Magn. Reson. 10 (1998) 331.
[18] J.P. Stamps, B. Ottink, J.M. Visser, J.P. van Duynhoven, R. Hulst, Difftrain: a novel approach to a true spectroscopic single-scan diffusion measurement, J. Magn. Reson. 151 (2001) 28.
[19] C. Buckley, K.G. Hollingsworth, A.J. Sederman, D.J. Holland, M.L. Johns, L.F. Gladden, Applications of fast diffusion measurement using Difftrain, J. Magn. Reson. 161 (2003) 112.
[20] L. Zha, I.J. Lowe, Optimized ultra-fast imaging sequence (OUFIS), Magn. Reson. Med. 33 (1995) 377.